

Gyrotropic Magnetic Effect in Black Phosphorus Irradiated with Bicircular Light

Fangyang Zhan,^{1,2} Xin Jin,³ Da-Shuai Ma,^{1,4} Jing Fan,⁵ Peng Yu,³ Dong-Hui Xu,^{1,4,*} and Rui Wang^{1,4,†}

¹*Institute for Structure and Function & Department of Physics & Chongqing Key Laboratory for Strongly Coupled Physics, Chongqing University, Chongqing 400044, P. R. China*

²*College of Mathematics and Statistics, Chongqing University, Chongqing 400044, P. R. China*

³*College of Physics and Electronic Engineering, Chongqing Normal University, Chongqing 400044, P. R. China*

⁴*Center of Quantum materials and devices, Chongqing University, Chongqing 400044, P. R. China*

⁵*Center for Computational Science and Engineering, Southern University of Science and Technology, Shenzhen 518055, P. R. China*

The gyrotropic magnetic effect, manifesting as a gyropropic current under a slowly-varying magnetic field, represents a fundamental property of Bloch electrons on the Fermi surface; however, it has not been observed in experiments. Here, we theoretically propose that Floquet engineering with bicircular light (BCL), which is a superposition of two opposite chiral waves of circularly polarized light with an integer frequency ratio, presents a fascinating strategy to generate and manipulate the gyrotropic magnetic effect in nodal line semimetals. The tailoring spatial symmetry of BCL irradiation can induce a topological transition from a nodal line semimetallic phase to a Weyl semimetallic phase characterized by a minimum number of misaligned Weyl nodes, resulting in the generation of gyrotropic current when a slowly oscillating magnetic field is applied. Moreover, using first-principles calculations, we show that the compressed black phosphorus under irradiation of BCL is an ideal candidate to realize the large gyropropic current with great advantages. Our work not only broadens potential candidate materials for achieving the experimentally accessible gyropropic current, but also provides deeper insights into the interplay between topological phenomena and light manipulation of symmetries.

Introduction. — Recent years have witnessed a surge of interest in topological semimetals due to their unique electronic band structures [1–6]. Arising from the interplay of symmetry and nontrivial band topology, conduction and valence bands in topological semimetals touch at discrete nodal points or along continuous nodal lines near the Fermi level. These topologically protected zero-dimensional pointlike or one-dimensional linelike Fermi surfaces give rise to many exotic quantum phenomena, including intriguing electromagnetic response and topological surface states [7–12]. Among various topological semimetals, of particular interest are Weyl semimetals (WSMs), in which the low-energy quasiparticles are described by massless chiral fermions, i.e., the right and left handed Weyl fermions. The presence of a nonorthogonal electric and magnetic field in WSMs can give rise to the so-called chiral magnetic effect (CME) [10, 13–15]. This effect roots in the chiral anomaly that was originally discussed in particle physics for Weyl fermions, as well as the Berry curvature surrounding Weyl nodes. Consequently, a nonequilibrium current aligned with the applied magnetic field occurs [10, 14, 16]. Based on CME, anomalous magnetotransport effects such as negative magnetoresistance have been observed in experimentally [8, 17–20].

In addition to the CME, another emergent effect was also proposed; that is, a time-dependent magnetic field can induce a current in inversion (P) symmetry broken WSMs, where Weyl nodes of opposite chirality are at different energies [21–23]. This effect can be considered as a manifestation of Faraday induction, linking to low-frequency limit of natural gyrotropy [24], and thus it is named as the gyrotropic magnetic effect (GME) [23]. Different from the CME, it was demonstrated that the GME is not governed by the chiral anomaly or Berry curvature, but by the intrinsic magnetic moment of Bloch electrons on the Fermi surface [22, 23]. The amplitude of a gyrotropic current arising from the GME is directly

proportional to the energy difference between right and left handed Weyl nodes [23], which provides a straightforward probe of chirality as it is a linear response.

The GME represents a basic property of Bloch electrons in a system with P -symmetry breaking, but both the theoretical and experimental investigations into this effect are relatively slow. To date, only a few WSMs have been theoretically predicted to exhibit the GME [22, 25, 26], with no experimental observations reported. The obstacle to measurements of GME possibly attributes to the fact that P -symmetry broken WSMs verified so far typically possess the time-reversal (T) symmetry. The combination of T -symmetry and additional crystalline symmetries (e.g., mirror symmetry) forces that the energy difference between Weyl nodes of opposite chirality are zero, naturally vanishing the gyrotropic current in these T -invariant WSMs. Previously, the predicted WSM SrSi_2 with T -symmetry but lacking mirror symmetry was proposed as a potential candidate for observing the GME [23]. However, the SrSi_2 compound possesses more than 60 Weyl nodes characterized by both linear and quadratic dispersions near the Fermi level [27], thus posing significant challenges for its experimental observation. To avoid such mishaps and ensure observing a visible gyrotropic current, it is highly desirable to design an ideal WSM state that only possesses a small number of Weyl nodes or especially one pair (a minimum number) of Weyl nodes near the Fermi level, with these Weyl nodes of opposite chirality exhibiting the sizable energy differences.

Recently, Floquet engineering has emerged as a promising approach for designing exotic topological states through the utilization of time-periodic light fields [28–36]. Periodic driving can effectively control the symmetry and topology of quantum materials. Various Floquet topological states have been proposed and even some of them have been confirmed in experiments [37–41]. The typical example is the Floquet WSM phase with flexibly controllable Weyl nodes, which can

be generated in topological insulators, Dirac semimetals, and nodal line semimetals (NLSMs) irradiated by circularly polarized light (CPL) [42–46]. More recently, employing irradiation of two-frequency bicircular light (BCL) with integer frequency ratio has been attracting a growing interest due to its enhancement of Floquet engineering capabilities [47–53]. Compared with monochromatic CPL irradiation, BCL irradiation can not only break T -symmetry but also selectively break spatial symmetries, including P -symmetry. This tailored symmetry opens a possible route to realize desirable topological states with unique properties (e.g., a minimum number of misaligned Weyl nodes), and thus investigate the GME current in BCL-irradiated materials.

Here, we propose that Floquet engineering with BCL irradiation offers a fascinating strategy to generate and control the GME current in NLSMs. Because of tailoring spatial symmetry through BCL irradiation, we emphasize that our proposal can be generally suit for both centrosymmetric and non-centrosymmetric systems. Starting from a low-energy effective model, we demonstrate that the polarization state of BCL leads to a topological phase transition from a NLSM state to a WSM state. Due to BCL irradiation breaking both P -symmetry and T -symmetry, the gapped NLSM can support a minimum number of misaligned Weyl nodes and thereby only one pair of Weyl nodes at different energies is present. Insights drawn from first-principles calculations in combination with the Floquet theory suggest that the compressed black phosphorus (BP) is an ideal candidate material to realize the GME. The compressed BP was demonstrated as a typical NLSM both in theories and experiments [54–56]. Under light irradiation, the energy and momentum separation between Weyl nodes of opposite chirality in compressed BP can be exactly controlled via manipulating the polarization state and amplitude of BCL, enabling the generation of a large gyrotropic current with great advantages. Due to the significant achievements in Floquet band engineering in BP [57, 58], our results are expected to be experimentally detected by laser-triggered photoconductive switch, which should draw extensive attention.

Symmetries broken in BCL irradiated nodal line.—To reveal the origin of gyrotropic current driven by BCL, we could start from a nodal ring system in the absence of the light field. Near the nodal line, the physics can be described by two-band Hamiltonian [59–61]:

$$H(\mathbf{k}) = P_k \sigma_z + Q_k \sigma_y \quad (1)$$

where $P_k = C - Bk^2$, $Q_k = vk_x + \lambda k_x^3$, and $k^2 = k_x^2 + k_y^2 + k_z^2$. B and C are model parameters, and v is the Fermi velocity along x direction. We can easily find that the presence of a nodal ring on the $k_x = 0$ plane is determined by the equation $k_y^2 + k_z^2 = C/B$ and protected by M_x mirror symmetry.

Further, considering the BCL irradiation generated by interferometrically combining a circularly polarized light (CPL) at frequency ω with its counter-rotating higher-harmonic $\eta\omega$. It

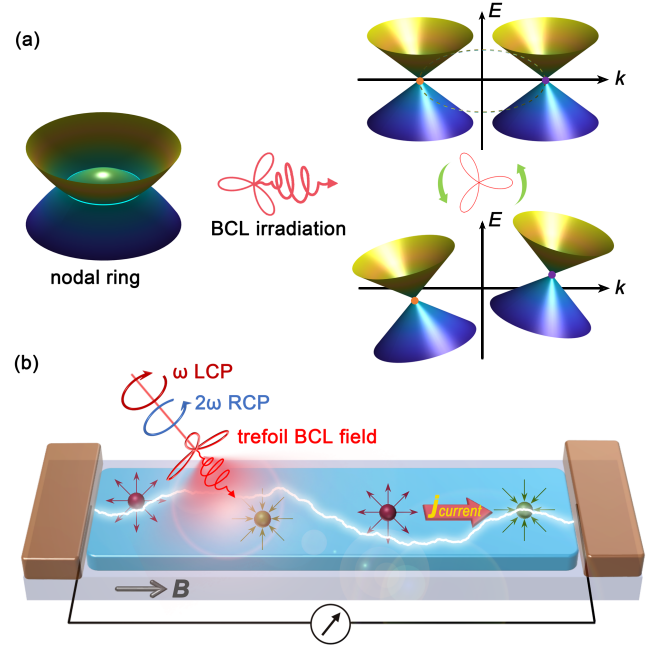


FIG. 1. The conceptual illustration of gyrotropic current driven by BCL. (a) Schematic dispersion relations for BCL drive phase transition from a NLSM state to a WSM state. The energy and momentum separation of opposite chiral Weyl nodes can be dynamically controlled via changing BCL polarization state. (b) The proposed setup for a gyrotropic current driven by trefoil BCL, which is the superposition of two opposite chirality CPL with different frequencies marked as ω and 2ω .

can be expressed as

$$\mathbf{A}(t) = A_0 \sqrt{2} \text{Re} [e^{-i(\eta\omega t - \alpha)} \boldsymbol{\varepsilon}_R + e^{-i\omega t} \boldsymbol{\varepsilon}_L], \quad (2)$$

where A_0 is amplitude of right-handed circularly polarized (RCP) and left-handed circularly polarized (LCP) light, $\boldsymbol{\varepsilon}_{R(L)}$ is RCP (LCP) light polarization basis vectors, η and α are respectively frequency ratio and phase difference between RCP and LCP light. For concreteness, in the following we focus on an effect of trefoil BCL ($\eta = 2$) irradiation. When a trefoil BCL field with polarization in xz plane is applied, the light can couple to the system via the minimal coupling substitution $H(\mathbf{k}, t) = H[\mathbf{k} + \mathbf{A}(t)]$. We note that it is necessary to include higher-order terms λk_x^3 in Q_k for the symmetries of the Floquet Hamiltonian to be consistent with those preserved by the light vector potential [49]. Here, we consider an off-resonant case in which the light frequency is significantly larger than the typical electronic transition energy. In this case, one can apply the high-frequency approximation and obtain a static effective Floquet-Bloch Hamiltonian [32, 49, 59, 62]:

$$H_{\text{eff}}(\mathbf{k}) = H^0(\mathbf{k}) + \sum_{n \geq 1} \frac{[H^n, H^{-n}]}{n\omega} + \mathcal{O}(\omega^{-2}), \quad (3)$$

$$= \tilde{P}_k \sigma_z + \tilde{Q}_k \sigma_y + \tilde{M}_k \sigma_x.$$

Here, $H^n(\mathbf{k}) = (1/T) \int_0^T dt e^{-in\omega t} H[\mathbf{k} + \mathbf{A}(t)]$ is the n th Fourier component of the time-dependent Hamiltonian, and

T is the period of light. \tilde{P}_k , \tilde{Q}_k , and \tilde{M}_k are the light renormalized Pauli matrix coefficients [see details in the Supplemental Material (SM) [63]]. Specially, the primary effect of the driving NLSM state to WSM state manifests in the $\tilde{M}_k \sigma_x$ term, $\tilde{M}_k = -iA_0^2 B [9A_0^2 \lambda k_z + 12A_0 \lambda k_x (k_x \sin \alpha + k_z \cos \alpha) + 4k_z (3\lambda k_x^2 + \nu)] / 2\omega$, which is absent in the original Hamiltonian [i.e., Eq. (1)]. This means that the momentum-dependent \tilde{M}_k can be controlled by polarization state of BCL, resulting in specific spatial symmetries broken. As shown in Fig. 1(a), when the relative phase α is set as 0 or π , the additional joint symmetry TM_x is imposed to the partner Weyl nodes with opposite chirality. Thus, these two symmetry-protected Weyl nodes are pinned at the same energy. For all other values of α , they reside at different energy and momentum space due to breaking of both P -symmetry and T -symmetry, resulting in the generation of gyrotropic current when a slowly oscillating magnetic field is applied [Fig. 1(b)].

Photoinduced gyrotropic current in the compressed BP. —

Next, we demonstrate the emergence of the gyrotropic current induced by BCL in compressed BP. As shown in Fig. 2(a), the bulk BP exhibits a van der Waals layered structure with alternately stacking order. Each layer is a honeycomb lattice which is puckered along the armchair direction. At ambient pressure, it is a monoatomic semiconductor with the narrow band gap of 0.3 eV [64, 65]. A compressive strain can induce an electronic topological transition from trivial semiconductor to nodal-ring semimetal, which has been experimentally accessible [55, 56]. Without loss of generality, we select a moderate 3.5% compressive strain along the armchair direction in our work. Because of the extremely weak spin-orbital coupling of the phosphorus element, the interplay between the spin-orbital coupling and light irradiation can be neglected. To investigate electronic and topological properties of compressed BP under CPL irradiation, we performed first-principles calculations within the framework of density-functional theory [66, 67]. By projecting plane waves onto localized Wannier basis, we investigated the light-driven band structures using the Wannier tight-binding Hamiltonian in combination with the Floquet theory. The calculated details are included in the SM [63].

Without light irradiation, compressed BP retains the same symmetry as the uncompressed case [68]. Near the Fermi level, two bands with opposite parity are inverted around the Z point [black solid line in Fig. 2(c)]. As a result, the nontrivial band topology can lead to the existence of a node ring in the Γ - Z - T plane of the Brillouin zone due to M_x symmetry, which is protected by the coexistence of P -symmetry and T -symmetry. As presented in Fig. 2(b), under irradiation by an off-resonant BCL field, where the polarized component of light is along the armchair direction, a light-driven topological transition occurs from NLSM to WSM, and this Floquet WSM phase only forms one pair of Weyl nodes. Figure 2(c) displays the band structures of compressed BP with different light intensities. One can find that the interplay between wavevector \mathbf{k} and light intensity can modify the electronic band structure. Once light intensity $eA_0/\hbar \neq 0 \text{ \AA}^{-1}$, the band structure imme-

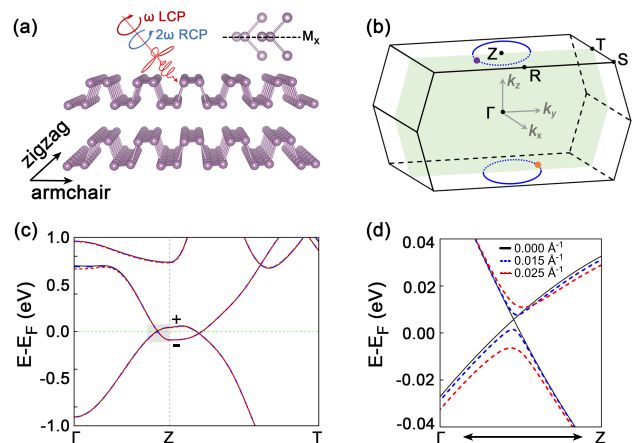


FIG. 2. BCL-dressed electronic structure evolution of compressed BP. (a) The atomic structure of BP and a schematic for irradiation of trefoil BCL field. (b) Brillouin zone of the bulk BP. The node ring (blue dotted line) is schematically shown in the Γ - Z - T plane. The light-driven a pair of Weyl nodes are represented by purple and orange dots respectively. (c) Evolution of electronic band structures of compressed BP under the irradiation of trefoil BCL perpendicular to xz plane. The top of the valence band and the bottom of the conduction band possess opposite eigenvalues. (d) The narrow energy window marked in (c) indicate that the initial band crossing is gapless, and the band gap is enlarged with an increase of light intensity.

diately becomes gapped except at the two Weyl nodes, and the band gap is enlarged with an increase of light intensity [see the locally enlarged view in Fig. 2(d)].

To further illustrate the unique ability of BCL, we provide the spatial trajectory of trefoil BCL for $\alpha = 0$ and $\pi/2$, as shown in Fig. 3(a). One can find that the TM_x symmetry is preserved only when one of the arms of the trefoil pattern aligns with the x axis ($\alpha = 0$ or π), thus governing two Weyl nodes with the same energy (see SM [63]). For all other values of α , irradiation with BCL can simultaneously destroy both P -symmetry and T -symmetry, leading to partner Weyl nodes with opposite chirality being separated both in energy and momentum. Figure 3(b) shows light-induced a pair of misaligned Weyl nodes (i.e., W^+ and W^-) when $\alpha = \pi/2$. We also calculate the evolution of Wannier charge center using the Wilson loop method [see the insets of Fig. 3(b)] to confirm its topological features.

In order to gain insight into the evolved behaviors of Weyl nodes under BCL field, we trace the position of Weyl nodes as function of α and light amplitude, and the results are shown in Fig. 3(c). For values of α varying from 0 to 2π , the Weyl nodes form closed trajectories in momentum space. The loop size expands as the light intensity increases, potentially allowing for the braiding of Weyl nodes through light stimulation. One significant consequence of the BCL-induced WSM phase in compressed BP is the existence of topologically protected surface states. To illustrate this nontrivial band topology, we calculate photon-dressed local density of states projected on the semi-infinite (100) surface based on the iterative Green's

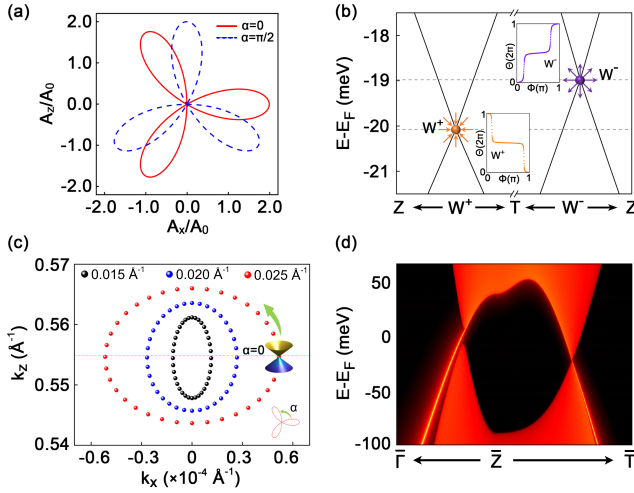


FIG. 3. BCL control of Weyl node locations in compressed BP. (a) The trefoil BCL polarization state for $\alpha = 0$ and $\pi/2$. (b) The enlarged view of band structure around two Weyl nodes is shown to emphasize the energy separation. The insets show the evolution of the Wannier charge centers around the W^+ and W^- , respectively. (c) Trajectory of the Weyl nodes (marked by the filled dots) in momentum space as α evolves from 0 to 2π by rotating the light waveform. (d) The calculated surface state projected on the semi-infinite (100) surface of compressed BP under the irradiation of BCL. We set the light intensity $eA_0/\hbar = 0.025 \text{ \AA}^{-1}$, and $\alpha = \pi/2$.

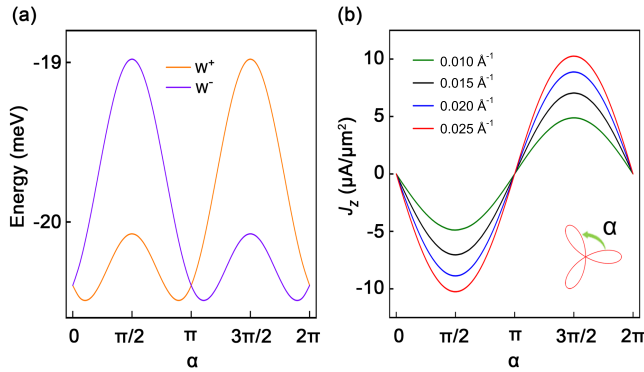


FIG. 4. The gyrotropic current induced by trefoil BCL in compressed BP. (a) The energy of Weyl nodes as a function of trefoil BCL orientation for light intensity $eA_0/\hbar = 0.025 \text{ \AA}^{-1}$. (b) The trefoil BCL-controlled electric current at different light intensities. We fix magnetic field in the z direction with amplitude of 3 T.

method using the Floquet Wannier tight-binding Hamiltonian. As shown in Fig. 3(d), we can see that a visible gap along $\bar{Z}-\bar{\Gamma}$ and a projected Weyl cone with linear dispersion along $\bar{Z}-\bar{T}$. Besides, we also provide the results on how the BCL irradiation affects the position of the Fermi arc under different light intensity in the SM [63].

Since spatial and magnetic symmetries strongly depend on the polarization state α of trefoil BCL, thus it can serve as a knob to dynamically control the energy separation between

this pair of Weyl nodes. Figure 4(a) exhibits clearly the α influence on the energy difference of Weyl nodes. Notably, the BCL-induced two Weyl nodes connected by TM_x symmetry have the degenerate energy when α equals 0 or π . For all other values of α , TM_x symmetry is not preserved, thus lifting the energy degeneracy of the Weyl nodes with opposite chirality. This BCL-driven symmetry modulation in BP is explicitly described in the previous low-energy effective model. More importantly, the energy difference of Weyl nodes directly reflects the degree of P -symmetry breaking. Owing to GME, one can precisely manipulate the gyrotropic current by applying a slowly oscillating magnetic field. To numerically simulate the BCL-driven current, we fix the magnetic field in z direction with amplitude of 3 T. As shown in Fig. 4(b), the current can be modulated by manipulating the polarization state and amplitude of trefoil BCL, thus achieving a continuous, wide-range, and switchable control of gyrotropic current in BP. Furthermore, the current in BCL-driven BP is predicted to lie within an experimentally accessible $\mu\text{A}/\mu\text{m}^2$ range when the light intensity $eA_0/\hbar = 0.01 \text{ \AA}^{-1}$ and polarization state $\alpha = \pi/2$, which is three orders of magnitude larger than that predicted in Cd_3As_2 [49].

Finally, in order to guide future experimental efforts to observe this effect, we evaluate the conditions needed and likelihood of success. In terms of the parameters for inducing the gyrotropic current, the pump photon energy and amplitude of the BCL are set as $\hbar\omega = 1 \text{ eV}$ and $eA_0/\hbar = 0.01 \text{ \AA}^{-1}$, corresponding to an electric field peak strength of $9.96 \times 10^7 \text{ V/m}$ (or energy density of $2.63 \times 10^9 \text{ W/cm}^2$). For a ultrafast laser pulse with a brief duration of 90 fs that is long enough to realize Floquet signatures with strong band renormalization in BP [57]. In this case, the laser fluence is only 0.24 mJ/cm^2 that is far below the damage threshold for laser ablation in BP [69], suggesting the energy deposition and heating effects are small. It is worth noting that there are inevitably the optical transitions and heating effects when the light field intensity increases, the gyrotropic current can still be detected in a lock-in type experiment, due spurious and heating effects are independent of α . Consequently, compressed BP driven by BCL may provide an unprecedented experimental advantages for exploring the gyrotropic current.

Summary.— In summary, based on the low-energy effective model and Floquet theory, we show that the polarization state of BCL provides an additional degree of freedom to selectively break spatial symmetries. From BCL-irradiated NLSMs, the tailoring symmetry provides a fascinating approach for achieving a desired WSM phase, which possesses a minimum number of Weyl nodes at different energies. Therefore, the photoinduced gyrotropic current is naturally present according to the GME if an additional slowly varying magnetic field is applied. This can be efficiently engineered by the polarization state and amplitude of BCL. As a concrete example, we show by first-principles calculations that the compressed BP is an ideal platform for realizing the BCL-induced GME. Remarkably, it is worth noting that the photoinduced gyrotropic current in the compressed BP is larger than that re-

cently predicted in Cd_3As_2 by three orders of magnitude [49], thus showing great advantages. We comprehensively evaluate the feasibility of the laser-pumping experiment, and the results indicate that the experiment was highly achievable. Benefiting from recently experimental progresses of Floquet band engineering in the BP [57, 58] and the NLSM phase verified in the compressed BP [54–56], the large gyrotropic current in the compressed BP would be expected to pose less challenges to experimental detection. Thus, our findings would draw extensive attention for exploring the GME in experiments. In addition, our work can also provide deeper insights into the interplay between topological phenomena and light-manipulated symmetries through Floquet engineering with BCL irradiation.

Acknowledgments. — This work was supported by the National Natural Science Foundation of China (NSFC, Grants No. 12204074, No. 12222402, No. 92365101, No. 12347101, and No. 12074108) and the Natural Science Foundation of Chongqing (Grants No. 2023NSCQ-JQX0024 and No. CSTB2022NSCQ-MSX0568). D.-S.M. also acknowledges funding from the China National Postdoctoral Program for Innovative Talent (Grant No. BX20220367) and the Project Funded by China Postdoctoral Science Foundation (Grant No. 2023M740411).

* donghuixu@cqu.edu.cn

† rcwang@cqu.edu.cn

- [1] M. Z. Hasan and C. L. Kane, Colloquium: Topological insulators, *Rev. Mod. Phys.* **82**, 3045 (2010).
- [2] X.-L. Qi and S.-C. Zhang, Topological insulators and superconductors, *Rev. Mod. Phys.* **83**, 1057 (2011).
- [3] N. P. Armitage, E. J. Mele, and A. Vishwanath, Weyl and Dirac semimetals in three-dimensional solids, *Rev. Mod. Phys.* **90**, 015001 (2018).
- [4] H. Gao, J. W. Venderbos, Y. Kim, and A. M. Rappe, Topological semimetals from first principles, *Annu. Rev. Mater. Res.* **49**, 153 (2019).
- [5] A. A. Burkov, Topological semimetals, *Nat. Mater.* **15**, 1145 (2016).
- [6] B. Q. Lv, T. Qian, and H. Ding, Experimental perspective on three-dimensional topological semimetals, *Rev. Mod. Phys.* **93**, 025002 (2021).
- [7] A. A. Zyuzin and A. A. Burkov, Topological response in Weyl semimetals and the chiral anomaly, *Phys. Rev. B* **86**, 115133 (2012).
- [8] X. Huang, L. Zhao, Y. Long, P. Wang, D. Chen, Z. Yang, H. Liang, M. Xue, H. Weng, Z. Fang, X. Dai, and G. Chen, Observation of the chiral-anomaly-induced negative magnetoresistance in 3D Weyl semimetal TaAs, *Phys. Rev. X* **5**, 031023 (2015).
- [9] E. Liu, Y. Sun, N. Kumar, L. Muechler, A. Sun, L. Jiao, S.-Y. Yang, D. Liu, A. Liang, Q. Xu, J. Kroder, V. Suess, H. Borrmann, C. Shekhar, Z. Wang, C. Xi, W. Wang, W. Schnelle, S. Wirth, Y. Chen, S. T. B. Goennenwein, and C. Felser, Giant anomalous Hall effect in a ferromagnetic kagome-lattice semimetal, *Nat. Phys.* **14**, 1125 (2018).
- [10] M. M. Vazifeh and M. Franz, Electromagnetic response of Weyl semimetals, *Phys. Rev. Lett.* **111**, 027201 (2013).
- [11] Y. Chen, S. Wu, and A. A. Burkov, Axion response in Weyl semimetals, *Phys. Rev. B* **88**, 125105 (2013).
- [12] X. Wan, A. M. Turner, A. Vishwanath, and S. Y. Savrasov, Topological semimetal and Fermi-arc surface states in the electronic structure of pyrochlore iridates, *Phys. Rev. B* **83**, 205101 (2011).
- [13] K. Fukushima, D. E. Kharzeev, and H. J. Warringa, Chiral magnetic effect, *Phys. Rev. D* **78**, 074033 (2008).
- [14] D. T. Son and N. Yamamoto, Berry curvature, triangle anomalies, and the chiral magnetic effect in Fermi liquids, *Phys. Rev. Lett.* **109**, 181602 (2012).
- [15] D. E. Kharzeev, The chiral magnetic effect and anomaly-induced transport, *Prog. Part. Nucl. Phys.* **75**, 133 (2014).
- [16] D. T. Son and B. Z. Spivak, Chiral anomaly and classical negative magnetoresistance of Weyl metals, *Phys. Rev. B* **88**, 104412 (2013).
- [17] J. Xiong, S. K. Kushwaha, T. Liang, J. W. Krizan, M. Hirschberger, W. Wang, R. J. Cava, and N. P. Ong, Evidence for the chiral anomaly in the Dirac semimetal Na_3Bi , *Science* **350**, 413 (2015).
- [18] C.-Z. Li, L.-X. Wang, H. Liu, J. Wang, Z.-M. Liao, and D.-P. Yu, Giant negative magnetoresistance induced by the chiral anomaly in individual Cd_3As_2 nanowires, *Nat. Commun.* **6**, 10137 (2015).
- [19] Q. Li, D. E. Kharzeev, C. Zhang, Y. Huang, I. Pletikoscic, A. V. Fedorov, R. D. Zhong, J. A. Schaefer, G. D. Gu, and T. Valla, Chiral magnetic effect in ZrTe_5 , *Nat. Phys.* **12**, 550–554 (2016).
- [20] F. Arnold, C. Shekhar, S.-C. Wu, Y. Sun, R. D. dos Reis, N. Kumar, M. Naumann, M. O. Ajeesh, M. Schmidt, A. G. Grushin, J. H. Bardarson, M. Baenitz, D. Sokolov, H. Borrmann, M. Nicklas, C. Felser, E. Hassinger, and B. Yan, Negative magnetoresistance without well-defined chirality in the Weyl semimetal TaP, *Nat. Commun.* **7**, 11615 (2016).
- [21] A. A. Zyuzin, S. Wu, and A. A. Burkov, Weyl semimetal with broken time reversal and inversion symmetries, *Phys. Rev. B* **85**, 165110 (2012).
- [22] P. Goswami, G. Sharma, and S. Tewari, Optical activity as a test for dynamic chiral magnetic effect of Weyl semimetals, *Phys. Rev. B* **92**, 161110 (2015).
- [23] S. Zhong, J. E. Moore, and I. Souza, Gyrotropic magnetic effect and the magnetic moment on the Fermi surface, *Phys. Rev. Lett.* **116**, 077201 (2016).
- [24] L. LANDAU and E. LIFSHITZ, *Electrodynamics of Continuous Media* (Pergamon Press, Oxford, 1984).
- [25] S. S. Tsirkin, P. A. Puente, and I. Souza, Gyrotropic effects in trigonal tellurium studied from first principles, *Phys. Rev. B* **97**, 035158 (2018).
- [26] J. Wang, B. Lian, and S.-C. Zhang, Generation of spin currents by magnetic field in T - and P -broken materials, *SPIN* **09**, 1940013 (2019).
- [27] S.-M. Huang, S.-Y. Xu, I. Belopolski, C.-C. Lee, G. Chang, T.-R. Chang, B. Wang, N. Alidoust, G. Bian, M. Neupane, D. Sanchez, H. Zheng, H.-T. Jeng, A. Bansil, T. Neupert, H. Lin, and M. Z. Hasan, New type of Weyl semimetal with quadratic double Weyl fermions, *Proc. Natl. Acad. Sci.* **113**, 1180 (2016).
- [28] C. Bao, P. Tang, D. Sun, and S. Zhou, Light-induced emergent phenomena in 2D materials and topological materials, *Nat. Rev. Phys.* **4**, 33 (2022).
- [29] T. Oka and S. Kitamura, Floquet engineering of quantum materials, *Annu. Rev. Condens. Matter Phys.* **10**, 387 (2019).
- [30] M. S. Rudner and N. H. Lindner, Band structure engineering and non-equilibrium dynamics in Floquet topological insula-

- tors, *Nat. Rev. Phys.* **2**, 229 (2020).
- [31] A. de la Torre, D. M. Kennes, M. Claassen, S. Gerber, J. W. McIver, and M. A. Sentef, Colloquium: Nonthermal pathways to ultrafast control in quantum materials, *Rev. Mod. Phys.* **93**, 041002 (2021).
- [32] T. Kitagawa, T. Oka, A. Brataas, L. Fu, and E. Demler, Transport properties of nonequilibrium systems under the application of light: Photoinduced quantum Hall insulators without Landau levels, *Phys. Rev. B* **84**, 235108 (2011).
- [33] M. Ezawa, Photoinduced topological phase transition and a single Dirac-cone state in Silicene, *Phys. Rev. Lett.* **110**, 026603 (2013).
- [34] H. Liu, H. Cao, and S. Meng, Floquet engineering of topological states in realistic quantum materials via light-matter interactions, *Prog. Surf. Sci.* **98**, 100705 (2023).
- [35] F. Zhan, Z. Ning, L.-Y. Gan, B. Zheng, J. Fan, and R. Wang, Floquet valley-polarized quantum anomalous Hall state in non-magnetic heterobilayers, *Phys. Rev. B* **105**, L081115 (2022).
- [36] F. Zhan, J. Zeng, Z. Chen, X. Jin, J. Fan, T. Chen, and R. Wang, Floquet engineering of nonequilibrium valley-polarized quantum anomalous Hall effect with tunable Chern number, *Nano Lett.* **23**, 2166 (2023).
- [37] Y. H. Wang, H. Steinberg, P. Jarillo-Herrero, and N. Gedik, Observation of Floquet-Bloch states on the surface of a topological insulator, *Science* **342**, 453 (2013).
- [38] S. Aeschlimann, S. A. Sato, R. Krause, M. Chávez-Cervantes, U. De Giovannini, H. Hübener, S. Forti, C. Coletti, K. Hanff, K. Rossnagel, A. Rubio, and I. Gierz, Survival of Floquet-Bloch states in the presence of scattering, *Nano Lett.* **21**, 5028 (2021).
- [39] D. Choi, M. Mogi, U. D. Giovannini, D. Azoury, B. Lv, Y. Su, H. Hübener, A. Rubio, and N. Gedik, *Direct observation of Floquet-Bloch states in monolayer graphene* (2024), arXiv:2404.14392 [cond-mat.mes-hall].
- [40] M. Merboldt, M. Schüler, D. Schmitt, J. P. Bange, W. Bennecke, K. Gadge, K. Pierz, H. W. Schumacher, D. Momeni, D. Steil, S. R. Manmana, M. Sentef, M. Reutz, and S. Mathias, *Observation of Floquet states in graphene* (2024), arXiv:2404.12791 [cond-mat.mes-hall].
- [41] Y. Li, Y. Yang, Y. Liu, J. Zhu, and K. Wu, Observation of Floquet states and their dephasing in colloidal nanoplatelets driven by visible pulses, *Nat. Photon.* **18**, 1044–1051 (2024).
- [42] R. Wang, B. Wang, R. Shen, L. Sheng, and D. Y. Xing, Floquet Weyl semimetal induced by off-resonant light, *EPL* **105**, 17004 (2014).
- [43] H. Liu, J.-T. Sun, and S. Meng, Engineering Dirac states in graphene: Coexisting type-I and type-II Floquet-Dirac fermions, *Phys. Rev. B* **99**, 075121 (2019).
- [44] A. Narayan, Tunable point nodes from line-node semimetals via application of light, *Phys. Rev. B* **94**, 041409 (2016).
- [45] T. Deng, B. Zheng, F. Zhan, J. Fan, X. Wu, and R. Wang, Photoinduced Floquet mixed-Weyl semimetallic phase in a carbon allotrope, *Phys. Rev. B* **102**, 201105 (2020).
- [46] M. Ezawa, Photoinduced topological phase transition from a crossing-line nodal semimetal to a multiple-Weyl semimetal, *Phys. Rev. B* **96**, 041205 (2017).
- [47] A. Kundu, H. A. Fertig, and B. Seradjeh, Floquet-engineered valleytronics in Dirac systems, *Phys. Rev. Lett.* **116**, 016802 (2016).
- [48] Y. Ikeda, S. Kitamura, and T. Morimoto, Photocurrent induced by a bicircular light drive in centrosymmetric systems, *Phys. Rev. Lett.* **131**, 096301 (2023).
- [49] T. V. Trevisan, P. V. Arribi, O. Heinonen, R.-J. Slager, and P. P. Orth, Bicircular light Floquet engineering of magnetic symmetry and topology and its application to the Dirac semimetal Cd_3As_2 , *Phys. Rev. Lett.* **128**, 066602 (2022).
- [50] A. Jimenez-Galan, R. E. F. Silva, O. Smirnova, and M. Ivanov, Lightwave control of topological properties in 2D materials for sub-cycle and non-resonant valley manipulation, *Nat. Photonics* **14**, 728 (2020).
- [51] X. Zhang, T. Carbin, A. B. Culver, K. Du, K. Wang, S.-W. Cheong, R. Roy, and A. Kogar, Light-induced electronic polarization in antiferromagnetic Cr_2O_3 , *Nat. Mater.* **23**, 460 (2024).
- [52] I. Tyulnev, Á. Jiménez-Galán, J. Poborska, L. Vamos, P. S. J. Russell, F. Tani, O. Smirnova, M. Ivanov, R. E. Silva, and J. Biegert, Valleytronics in bulk MoS_2 with a topologic optical field, *Nature* **628**, 746 (2024).
- [53] S. Mitra, A. Jimenez-Galan, M. Aulich, M. Neuhaus, R. E. F. Silva, V. Pervak, M. F. Kling, and S. Biswas, Light-wave-controlled Haldane model in monolayer hexagonal boron nitride, *Nature* **628**, 752 (2024).
- [54] J. Zhao, R. Yu, H. Weng, and Z. Fang, Topological node-line semimetal in compressed black phosphorus, *Phys. Rev. B* **94**, 195104 (2016).
- [55] Z. J. Xiang, G. J. Ye, C. Shang, B. Lei, N. Z. Wang, K. S. Yang, D. Y. Liu, F. B. Meng, X. G. Luo, L. J. Zou, Z. Sun, Y. Zhang, and X. H. Chen, Pressure-induced electronic transition in black phosphorus, *Phys. Rev. Lett.* **115**, 186403 (2015).
- [56] K. Akiba, Y. Akahama, M. Tokunaga, and T. C. Kobayashi, Realization of nodal-ring semimetal in pressurized black phosphorus, *Phys. Rev. B* **109**, L201103 (2024).
- [57] S. Zhou, C. Bao, B. Fan, H. Zhou, Q. Gao, H. Zhong, T. Lin, H. Liu, P. Yu, P. Tang, S. Meng, W. Duan, and S. Zhou, Pseudospin-selective Floquet band engineering in black phosphorus, *Nature* **614**, 75 (2023).
- [58] S. Zhou, C. Bao, B. Fan, F. Wang, H. Zhong, H. Zhang, P. Tang, W. Duan, and S. Zhou, Floquet engineering of black phosphorus upon below-gap pumping, *Phys. Rev. Lett.* **131**, 116401 (2023).
- [59] Z. Yan and Z. Wang, Tunable Weyl points in periodically driven nodal line semimetals, *Phys. Rev. Lett.* **117**, 087402 (2016).
- [60] Y. Kim, B. J. Wieder, C. L. Kane, and A. M. Rappe, Dirac line nodes in inversion-symmetric crystals, *Phys. Rev. Lett.* **115**, 036806 (2015).
- [61] C. Fang, Y. Chen, H.-Y. Kee, and L. Fu, Topological nodal line semimetals with and without spin-orbital coupling, *Phys. Rev. B* **92**, 081201 (2015).
- [62] T. Mikami, S. Kitamura, K. Yasuda, N. Tsuji, T. Oka, and H. Aoki, Brillouin-wigner theory for high-frequency expansion in periodically driven systems: Application to Floquet topological insulators, *Phys. Rev. B* **93**, 144307 (2016).
- [63] See Supplemental Material for detailed computational methods of first-principles calculations, the effective low energy time-independent Hamiltonian, and the topological phase transition in BP irradiated with CPL and BCL, which include Refs. [70–80].
- [64] Y. Akahama, S. Endo, and S.-i. Narita, Electrical properties of black phosphorus single crystals, *J. Phys. Soc. Jpn.* **52**, 2148 (1983).
- [65] H. Liu, A. T. Neal, Z. Zhu, Z. Luo, X. Xu, D. Tománek, and P. D. Ye, Phosphorene: An unexplored 2D semiconductor with a high hole mobility, *ACS Nano* **8**, 4033 (2014).
- [66] P. Hohenberg and W. Kohn, Inhomogeneous electron gas, *Phys. Rev.* **136**, B864 (1964).
- [67] W. Kohn and L. J. Sham, Self-consistent equations including exchange and correlation effects, *Phys. Rev.* **140**, A1133 (1965).
- [68] M. Okajima, S. Endo, Y. Akahama, and S. ichiro Narita, Electric-

- cal investigation of phase transition in black phosphorus under high pressure, *Jpn. J. Appl. Phys.* **23**, 15 (1984).
- [69] G. Qiu, Q. Nian, M. Motlag, S. Jin, B. Deng, Y. Deng, A. R. Charnas, P. D. Ye, and G. J. Cheng, Ultrafast laser-shock-induced confined metaphase transformation for direct writing of black phosphorus thin films, *Adv. Mater.* **30**, 1704405 (2018).
- [70] G. Kresse and J. Furthmüller, Efficient iterative schemes for ab initio total-energy calculations using a plane-wave basis set, *Phys. Rev. B* **54**, 11169 (1996).
- [71] A. A. Mostofi, J. R. Yates, G. Pizzi, Y.-S. Lee, I. Souza, D. Vanderbilt, and N. Marzari, An updated version of Wannier90: A tool for obtaining maximally-localised wannier functions, *Comput. Phys. Commun.* **185**, 2309 (2014).
- [72] M. P. L. Sancho, J. M. L. Sancho, J. M. L. Sancho, and J. Rubio, Highly convergent schemes for the calculation of bulk and surface green functions, *J. Phys. F: Met. Phys* **15**, 851 (1985).
- [73] Q. Wu, S. Zhang, H.-F. Song, M. Troyer, and A. A. Soluyanov, Wanniertools : An open-source software package for novel topological materials, *Comput. Phys. Commun.* **224**, 405 (2018).
- [74] L. A. Burns, Á. V. Mayagoitia, B. G. Sumpter, and C. D. Sherrill, Density-functional approaches to noncovalent interactions: A comparison of dispersion corrections (DFT-D), exchange-hole dipole moment (XDM) theory, and specialized functionals, *J. Chem. Phys.* **134**, 084107 (2011).
- [75] K. F. Milfeld and R. E. Wyatt, Study, extension, and application of Floquet theory for quantum molecular systems in an oscillating field, *Phys. Rev. A* **27**, 72 (1983).
- [76] A. Gómez-León and G. Platero, Floquet-Bloch theory and topology in periodically driven lattices, *Phys. Rev. Lett.* **110**, 200403 (2013).
- [77] J. H. Shirley, Solution of the Schrödinger equation with a Hamiltonian periodic in time, *Phys. Rev.* **138**, B979 (1965).
- [78] D. H. Dunlap and V. M. Kenkre, Dynamic localization of a charged particle moving under the influence of an electric field, *Phys. Rev. B* **34**, 3625 (1986).
- [79] H. Sambe, Steady states and quasienergies of a quantum-mechanical system in an oscillating field, *Phys. Rev. A* **7**, 2203 (1973).
- [80] F. Gesztesy and H. Mitter, A note on quasi-periodic states, *J. Phys. A: Math. Gen.* **14**, L79 (1981).